

**POLYBENZOXAZINE-BASED CARBON AEROGELS
FOR CARBON DIOXIDE CAPTURE**

Nittada Jungsawat

A Thesis Submitted in Partial Fulfillment of the Requirements
for the Degree of Master of Science
The Petroleum and Petrochemical College, Chulalongkorn University
in Academic Partnership with
The University of Michigan, The University of Oklahoma,
Case Western Reserve University and Institut Français du Pétrole
2015


I28368691

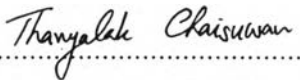
Thesis Title: Polybenzoxazine-based Carbon Aerogels for Carbon Dioxide Capture
By: Nittada Jungsawat
Program: Petroleum Technology
Thesis Advisors: Dr. Uthaiporn Suriyaphadilok
Asst. Prof. Thanyalak Chaisuwan

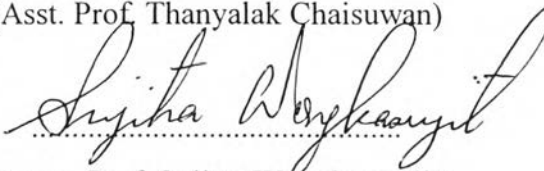
Accepted by The Petroleum and Petrochemical College, Chulalongkorn University, in partial fulfillment of the requirements for the Degree of Master of Science.

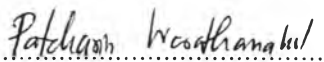

..... College Dean
(Asst. Prof. Pomthong Malakul)

Thesis Committee:


.....
(Dr. Uthaiporn Suriyaphadilok)


.....
(Asst. Prof. Thanyalak Chaisuwan)


.....
(Assoc. Prof. Sujitra Wongkasemjit)


.....
(Assoc. Prof. Patcharin Worathanakul)

ABSTRACT

5673016063 : Petroleum Technology Program

Nittada Jungsawat: Polybenzoxazine-based Carbon Aerogels for CO₂ Capture.

Thesis Advisors: Dr. Uthaiporn Suriyaphadilok, and Asst. Prof. Thanyalak Chaisuwan 209 pp.

Keywords : Benzoxazine/ Polybenzoxazine aerogel/ Carbon aerogel/ CO₂ capture

Carbon aerogels developed from a new type of phenolic resin, called polybenzoxazine, was considered to be used as an adsorbent for CO₂ adsorption application. In particular, phenol-based PBZs from two different types of amine precursors (i.e., diethylenetriamine (DETA) and pentaethylenehexamine (PEHA)) were synthesized by a sol-gel technique, followed by carbonization in nitrogen and activation with CO₂. Several techniques such as FTIR, DSC, TGA, sorptomatic analyser, CHN, and XPS have been employed to characterize the textural properties, porosity, nitrogen content, and other adsorbent properties on the adsorption performance. The CO₂ adsorption capacity of these adsorbents was measured using a simultaneous thermal analyzer (STA) at atmospheric pressure and adsorption temperatures of 40 °C, 75 °C, and 110 °C. The concentrations of benzoxazine monomer were varied at 30, 35, and 40 wt% in order to tune the surface properties of these porous PBZ aerogels. The effects of different amine chain lengths and loading PEG-PPG-PEG block copolymer as non-ionic surfactant on aerogel materials were investigated. The CO₂ adsorption performance at all adsorption conditions of DETA-derived PBZ carbon aerogels performed higher than PEHA-derived PBZ carbon aerogels due to a larger surface area and a higher pore volume; moreover, both types of carbon aerogels exhibited higher CO₂ adsorption capacity compared to those activated carbons from PBZ prepared by bulk polymerization. Furthermore, 30 wt% DETA-based carbon aerogel at activating temperature of 900 °C provided the highest CO₂ uptake at 1.79 mmol_{CO₂}/g_{adsorbent} at adsorption condition of 40 °C and 1 bar.

บทคัดย่อ

นิตดา จึงสวัสดิ์: พอลิเบนซอกซาซีนคาร์บอนแอโรเจลสำหรับการดูดซับก๊าซคาร์บอนไดออกไซด์ (Polybenzoxazine-based Carbon Aerogels for Carbon Dioxide Capture) อ.ที่ปรึกษา: ดร. อุทัยพร สุริยประภาติก และผู้ช่วยศาสตราจารย์ ดร. ธัญญลักษณ์ ฉายสุวรรณ 209 หน้า

คาร์บอนแอโรเจลพัฒนามาจากเรซินชนิดใหม่ของพีนอลิกเรซิน ที่เรียกว่าพอลิเบนซอกซาซีน ได้รับการพิจารณาให้เป็นตัวดูดซับ สำหรับการประยุกต์ใช้ในการดูดซับก๊าซคาร์บอนไดออกไซด์ โดยเฉพาะอย่างยิ่งพอลิเบนซอกซาซีนสังเคราะห์จากพีนอล ที่ใช้เอมีนสองชนิดที่ต่างกัน (อันได้แก่ ไดเอทิลีนไตรเอมีน และเพนตะเอทิลีนเฮกซามีน) ถูกสังเคราะห์ด้วยวิธีโซลเจล ต่อจากนั้นจะถูกเปลี่ยนรูปให้เป็นคาร์บอนภายใต้อุณหภูมิสูงในสภาวะบรรยากาศของไนโตรเจนและถูกกระตุ้นภายใต้สภาวะบรรยากาศของคาร์บอนไดออกไซด์ เทคนิคหลายอย่างอันได้แก่ ฟลูเรียทรานฟอร์มอินฟราเรดสเปกโตรมิเตอร์ ดิฟเฟอเรนเชียลสแกนนิ่งแคลอริมิเตอร์ เทคนิคเทอร์โมกราวิเมตริกอะนาไลซิส เครื่องมือวิเคราะห์พื้นที่ผิวของวัสดุที่มีความพรุน เครื่องมือวิเคราะห์องค์ประกอบของธาตุ (อันได้แก่ คาร์บอน ไฮโดรเจน และไนโตรเจน) และเอ็กซ์เรย์โฟโตอิเล็กตรอนสเปกโตรสโคปี ได้ถูกใช้ในการวิเคราะห์คุณสมบัติต่างๆที่เกี่ยวข้องกับความสามารถในการดูดซับ สมรรถนะของตัวดูดซับทั้งหลายถูกวิเคราะห์ผ่านเครื่องมือวิเคราะห์เทอร์โมกราวิเมตริกอะนาไลซิสที่ความดันบรรยากาศและอุณหภูมิต่างๆ อันได้แก่ 40 75 และ 110 องศาเซลเซียส ในงานวิจัยนี้ความเข้มข้นของเบนซอกซาซีน โมโนเมอร์ถูกศึกษาที่ความเข้มข้น 30 35 และ 40 เปอร์เซ็นต์โดยน้ำหนัก เพื่อปรับเปลี่ยนตามขนาดพื้นที่ผิวและสมบัติทางรูพรุนต่างๆ ของพอลิเบนซอกซาซีนที่มีรูพรุน รวมถึงการศึกษาอิทธิพลของความยาวของสายโซ่เอมีน และการเติมสารลดแรงตึงผิวชนิดไม่มีไอออนต่อวัสดุแอโรเจล ประสิทธิภาพของการดูดซับคาร์บอนไดออกไซด์ในทุกสภาวะของการดูดซับของคาร์บอนแอโรเจลจากสารตั้งต้นของไดเอทิลีนไตรเอมีนแสดงค่าสูงกว่าแอโรเจลจากสารตั้งต้นของเพนตะเอทิลีนเฮกซามีน เนื่องจากพื้นที่ผิวที่มากกว่าและปริมาณรูพรุนที่เยอะกว่า นอกจากนี้คาร์บอนแอโรเจลจากเอมีนทั้งสองชนิดแสดงถึงประสิทธิภาพของการดูดซับคาร์บอนไดออกไซด์ที่สูงกว่าเมื่อเทียบกับถ่านกัมมันต์จากพอลิเบนซอกซาซีนที่เตรียมโดยวิธีบัลค์พอลิเมอไรเซชัน ยิ่งกว่านั้นคาร์บอนแอโรเจลจากสารตั้งต้นของไดเอทิลีนไตรเอมีนที่เตรียมจากโมโนเมอร์ที่ความเข้มข้น 30 เปอร์เซ็นต์โดยน้ำหนักแสดงค่าความสามารถในการดูดซับก๊าซคาร์บอนไดออกไซด์สูงที่สุดที่ 1.79 มิลลิโมลของก๊าซคาร์บอนไดออกไซด์ต่อกรัมของตัวดูดซับ ภายใต้สภาวะการดูดซับที่ 40 องศาเซลเซียสและ 1 บาร์

ACKNOWLEDGEMENTS

I would like to express my special appreciation and deep appreciation to my advisor and co advisor, Dr. Uthaiporn Suriyaphādilok and Asst. Prof. Thanyalak Chaisuwan, for their kindness, valuable guidance, and encouragement throughout this research.

I would also like to thank my committee members, Assoc. Prof. Sujitra Wongkasemjit and Assoc. Prof. Patcharin Worathanakul for serving as my committee members even at hardship.

I would like to thank Assoc. Prof. Boonyarach Kitiyanan for supporting the carbonization reactor.

This thesis work is funded by The Petroleum and Petrochemical College; and The Nation Center of Excellence for Petroleum, Petrochemicals, and Advanced Materials, Thailand.

I would like to thank the entire faculty and staff at The Petroleum and Petrochemical College, Chulalongkorn University for their kind assistance and cooperation. This research work was partially supported by the Ratchadaphisek Somphot Endowment Fund (2013), Chulalongkorn University (CU-56-900-FC), Thailand Research Fund (IRG5780012).

Finally, it is also a pleasure to acknowledge my family for their love, understanding, encouragement, and the constant inspiration throughout my study.

TABLE OF CONTENTS

	PAGE
Title Page	i
Abstract (in English)	iii
Abstract (in Thai)	iv
Acknowledgements	v
Table of Contents	vi
List of Tables	xi
List of Figures	xiii
CHAPTER	
I INTRODUCTION	1
II LITERATURE REVIEW	4
2.1 Carbon Dioxide (CO ₂) and Climate Change	4
2.2 CO ₂ Capture and Separation	6
2.2.1 Post-combustion	6
2.2.2 Pre-combustion	7
2.2.3 Oxy-combustion	8
2.3 Adsorption	8
2.3.1 Thermal Swing Adsorption (TSA)	9
2.3.2 Vacuum Swing Adsorption (VSA)	9
2.3.3 Pressure Swing Adsorption (PSA)	9
2.3.4 Electrical Swing Adsorption (ESA)	9
2.4 Porous Materials	11
2.5 Adsorbent	16
2.5.1 Silica	17
2.5.2 Activated Carbon	19
2.5.3 Polymer-Based Compounds	23
2.6 Polybenzoxazine	25

CHAPTER	PAGE
2.6.1	Foaming Technique 28
2.6.2	A Sol-gel Technique 32
2.7	Adsorption Measurement 35
2.7.1	Gravimetric Method 35
2.7.2	Temperature Programmed Desorption (TPD) 35
2.7.3	Volumetric Method 36
III	EXPERIMENTAL 41
3.1	Materials and Equipment 41
3.1.1	Materials and Chemicals 41
3.1.2	Equipment 41
3.2	Experimental Procedures 42
3.2.1	Preparation of Benzoxazine Monomer 42
3.2.2	Preparation of Polybenzoxazine Aerogel 42
3.2.3	Preparation of PBZ Aerogel Loading with Non-ionic Surfactant 43
3.2.4	Preparation of Carbon Aerogel or Activated Carbon from PBZ 43
3.3	Characterizations of Benzoxazine and Adsorbents-derived from PBZ 43
3.3.1	Fourier Transform Infrared Spectrometer (FTIR) 43
3.3.2	Differential Scanning Calorimeter (DSC) 44
3.3.3	Thermogravimetric Analysis (TGA) 44
3.3.4	Surface Area Analyzer (Sorptomatic) 44
3.3.5	CHN Analyzer 45
3.3.6	X-ray Photoelectron Spectroscopy (XPS) 45
3.3.7	Scanning Electron Microscope (SEM) 45
3.4	Adsorption Measurement 47
3.4.1	Pressure Decay Method 47
3.4.2	Gravimetric Method 49

CHAPTER	PAGE
IV RESULTS AND DISCUSSION (SYNTHESIS AND CHARACTERIZATION OF POLYBENZOXAZINE)	50
4.1 Characterization of Materials	50
4.1.1 Characterization of Benzoxazine Monomer	50
4.1.2 Characterization of Polybenzoxazine	54
4.2 Effect of Preparation Method on Polybenzoxazine-based Carbon	66
4.3 Effect of Benzoxazine Monomer Concentrations on Polybenzoxazine-based Organic Aerogels and Carbon Aerogels	68
4.4 Effect of Chain Lengths of Amine Precursors on Activated Carbons from Polybenzoxazine and Polybenzoxazine-based Carbon Aerogels	73
4.5 Effect of Activation Temperatures on Activated Carbon from Polybenzoxazine and Polybenzoxazine-based Carbon Aerogel	74
4.6 Effect of Non-Ionic Surfactant (PEG-PPG-PEG Block Copolymer) on Polybenzoxazine-based Carbon Aerogel	76
V RESULTS AND DISCUSSION (CARBON MATERIALS FROM POLYBENZOXAZINE FOR CARBON DIOXIDE ADSORPTION APPLICATION)	78
5.1 Characterization of Adsorbents	78
5.1.1 Adsorbents Characterization	78
5.1.2 Ultimate Analysis	83
5.1.3 Surface Analysis by XPS	85
5.2 Effect of Preparation Method on CO ₂ Adsorption Performance	93
5.3 Effect of Benzoxazine Concentrations on CO ₂ Adsorption Performance	95

CHAPTER	PAGE
5.4 Effect of Chain Lengths of Amine Precursors on CO ₂ Adsorption Performance	97
5.5 Effect of Activation Temperatures of Carbon Aerogels on CO ₂ Adsorption Performance	99
5.6 Effect of Non-ionic Surfactant (PEG-PPG-PEG Block Copolymer) in Polybenzoxazine-based Carbon Aerogel on CO ₂ Adsorption Performance	100
5.7 Effect of Adsorption Temperatures on CO ₂ Adsorption Performance	102
5.8 Effect of Regenerations on Carbon Materials	104
VI CONCLUSIONS AND RECOMMENDATIONS	111
6.1 Conclusions (Synthesis and Characterization of Polybenzoxazine)	111
6.2 Conclusions (Carbon Materials from Polybenzoxazine for Carbon Dioxide Adsorption Application)	112
6.3 Recommendations	113
REFERENCES	114
APPENDICES	122
Appendix A Calculation for Benzoxazine Synthesis Ratio	122
Appendix B FTIR Spectra of Benzoxazine Monomers and Polybenzoxazines	124
Appendix C DSC Thermograms of all Materials	126
Appendix D TGA Thermograms of all Materials	130
Appendix E Calculation for Residual Weight of Polybenzoxazine	133
Appendix F %Burn Off of Carbon Aerogels from Polybenzoxazine	135

CHAPTER	PAGE
Appendix G XPS Spectra of all Materials	136
Appendix H Isotherm, BJH Pore Size Distribution, and HK Pore Size Distribution of all Adsorbents	169
Appendix I Adsorption/Desorption Isotherms of all Materials	198
Appendix J SEM Images of all Materials	205
CURRICULUM VITAE	209

LIST OF TABLES

TABLE		PAGE
2.1	Global warming potential over 100 years on a per molecule basis	4
2.2	Advantages and disadvantages of post-combustion	7
2.3	Advantages and disadvantages of pre-combustion	7
2.4	Comparison between physisorption and chemisorptions	11
2.5	Representative properties of commercial porous adsorbents	17
2.6	The synthesis and pore size diameter of polybenzoxazine foam	31
2.7	The synthesis and pore size diameter of porous polybenzoxazine	34
4.1	The surface property of organic PBZ aerogels derived from DETA and PEHA at different PBZ concentration and their carbon aerogels obtaining at activation temperature of 800 °C	64
4.2	The surface property of activated carbon from polybenzoxazine, carbon aerogels, and carbon aerogels containing with non-organic surfactant (P ₁₂₃) at activation temperature of 900 °C	65
5.1	The surface property of activated carbon from polybenzoxazine, a series of organic aerogels and carbon aerogels at activation temperature of 800 °C	81
5.2	The surface property of activated carbon from polybenzoxazine, carbon aerogels, and carbon aerogels containing with non-organic surfactant (P ₁₂₃) at activation temperature of 900 °C	82
5.3	Ultimate analysis of all materials	84
5.4	Deconvolution results of polybenzoxazine and PBZ-based organic aerogels by DETA as precursor	87
5.5	Deconvolution results of polybenzoxazine and PBZ-based organic aerogels by PEHA as precursor	88
5.6	Deconvolution results of activated carbon from PBZ and carbon aerogels from derived PBZ by DETA as precursor	89
5.7	Deconvolution results of activated carbon from PBZ and carbon aerogels from derived PBZ by PEHA as precursor	90

TABLE	PAGE
5.8 · Deconvolution results of carbon materials by DETA as precursor at activation temperature of 900 °C	91
5.9 Deconvolution results of carbon materials by PEHA as precursor at activation temperature of 900 °C	92
5.10 Assignments of deconvoluted peaks as characterized by XPS	93
5.11 The CO ₂ adsorption performances of activated carbons and organic aerogels from PBZ at different adsorption temperatures of 40, 75, and 110 °C and 1 bar	103
5.12 The CO ₂ adsorption performances of carbon materials from PBZ at different adsorption temperatures of 40, 75, and 110 °C and 1 bar	103
5.13 The regeneration percentages of activated carbons from PBZ, carbon aerogels at different monomer concentrations of 30, 35, and 40 wt% by DETA and PEHA as amine precursors at desorption temperatures of 40 and 75 °C (all these carbon materials were activated at 800 °C)	105
5.14 The regeneration percentages of activated carbons from PBZ, carbon aerogels at different monomer concentrations of 30, 35, and 40 wt% by DETA and PEHA as amine precursors at desorption temperature of 110 °C (all these carbon materials were activated at 800 °C)	106
5.15 The regeneration percentages of activated carbons from PBZ, carbon aerogels from 30 wt% of benzoxazine solution, and carbon aerogels from 30 wt% of benzoxazine solution with non-ionic surfactant by DETA and PEHA as reactants at desorption temperatures of 40, 75, and 110 °C (all these carbon materials were activated at 900 °C)	107
F1 Comparison of %burn off of PBZ-derived carbon aerogels from two instruments (TG-DTA and Furnace)	135

LIST OF FIGURES

FIGURE	PAGE
2.1 Global CO ₂ emissions by source: Baseline, 1980-2050.	5
2.2 The different routes for CO ₂ capture and separation.	6
2.3 The CO ₂ adsorption behavior on the adsorbent surface.	8
2.4 The physisorption of CO ₂ and the chemisorption of CO ₂ on porous substrate.	9
2.5 a) A microporous material, b) A mesoporous material, and c) A macroporous material.	12
2.6 The different types of pores.	13
2.7 The structure of DETA, PEHA and PEI.	22
2.8 The structure of TEA, AMPD and DIPA.	23
2.9 Monofunctional benzoxazine monomer synthesis.	26
2.10 Bifunctional benzoxazine monomer synthesis.	26
2.11 The microscopic images of polybenzoxazine foam (a) and carbon foam (b) at 10 wt% of AZD.	29
2.12 The microscopic images of polybenzoxazine foams at several relative densities (a) 0.35, (b) 0.43, (c) 0.50 and (d) 0.60.	30
2.13 Synthesis of diphenolic acid benzoxazine.	31
2.14 Cell size distribution and microscopic image of diphenolic acid benzoxazine foam at foaming temperature of 190 °C.	31
2.15 Schematic of the volumetric differential pressure hydrogen adsorption apparatus.	37
3.1 The polybenzoxazine synthesis reactions (a) Polybenzoxazine-based on DETA and (b) Polybenzoxazine based on PEHA.	46
3.2 Schematic diagram of the adsorption system.	48
4.1 FT-IR spectrum of the benzoxazine monomer by DETA as reactant.	51
4.2 FT-IR spectrum of the benzoxazine monomer by PEHA as reactant.	51
4.3 DSC thermograms of benzoxazine monomers by DETA and PEHA as reactants.	52

FIGURE	PAGE
4.4 TGA thermograms of benzoxazine monomers with DETA and PEHA as amine reactants.	53
4.5 FT-IR spectrum of polybenzoxazine by DETA as reactant.	54
4.6 FT-IR spectrum of polybenzoxazine by PEHA as reactant.	55
4.7 DSC thermograms of polybenzoxazines by DETA and PEHA as reactant.	56
4.8 DSC thermograms of (a) DETA-40wt% derived aerogel at 180 °C for 15 min, (b) DETA-40wt% derived aerogel at 180 °C for 30 min, and (c) DETA-40wt% derived aerogel at 180 °C for 45 min.	57
4.9 DSC thermograms of polybenzoxazine aerogels before curing step with DETA as reactant.	58
4.10 DSC thermograms of polybenzoxazine aerogels after curing step with DETA as reactant.	58
4.11 DSC thermograms of polybenzoxazine aerogels before curing step with PEHA as reactant.	59
4.12 DSC thermograms of polybenzoxazine aerogels after curing step with PEHA as reactant.	60
4.13 TGA thermograms of polybenzoxazine and polybenzoxazine aerogels with DETA as reactant.	61
4.14 TGA thermograms of polybenzoxazine and polybenzoxazine aerogels with PEHA as reactant.	61
4.15 TGA thermograms of PBZs derived from DETA and PEHA after heating up to 900 °C (with a heating rate of 20 °C/min).	62
4.16 TGA thermograms of PEG-PPG-PEG block copolymer after heating up to 900 °C (with heating rate of 20 °C/min).	63
4.17 TGA thermograms of PBZ aerogels derived from DETA and PEHA with and without non-ionic surfactant (PEG-PPG-PEG block copolymer) after heating up to 900 °C (with heating rate of 20 °C/min).	64

FIGURE	PAGE
4.18 SEM images of (a) activated carbon from DETA-derived PBZ, (b) activated carbon from PEHA-derived PBZ, (c) carbon aerogel from DETA-30wt%, and (d) carbon aerogel from PEHA-30wt%.	67
4.19 SEM images of (a) fully cured DETA-derived PBZ aerogel at 20 wt%, (b) 25 wt%, and (c) 30 wt% of monomer solutions.	69
4.20 SEM images of (a) DETA-derived PBZ carbon aerogel at 30 wt%, (b) 30 wt%, (c) 35 wt%, (d) 35 wt%, (e) 40 wt%, and (f) 40 wt% of monomer solutions; low magnification for (a), (c), and (e); high magnification for (b), (d), and (f).	71
4.21 SEM images of (a) PEHA-derived PBZ carbon aerogel at 30 wt%, (b) 30 wt%, (c) 35wt%, (d) 35 wt%, (e) 40 wt%, and (f) 40 wt% of monomer solutions; low magnification for (a), (c), and (e); high magnification for (b), (d), and (f).	72
4.22 SEM images of (a) activated carbon from DETA-derived PBZ, (b) activated carbon from PEHA-derived PBZ with a magnification of 5,000 times.	73
4.23 SEM images of (a) carbon aerogel from DETA-30 wt% at activation temperature of 800 °C, (b) carbon aerogel from DETA-30 wt% at activation temperature of 900 °C, (c) carbon aerogel from PEHA-30 wt% at activation temperature of 800 °C, and (d) carbon aerogel from PEHA-30 wt% at activation temperature of 900 °C.	75
5.1 SEM images of (a) activated carbon from DETA-derived PBZ, (b) activated carbon from PEHA-derived PBZ with a magnification of 2,000 times.	79
5.2 SEM images of (a) PEHA-derived PBZ carbon aerogel at 30 wt%, (b) 35 wt%, and (c) 40 wt% of monomer solutions with magnification of 600 times.	80
5.3 The chemical structures of (a) DETA-derived polybenzoxazine and (b) PEHA-derived polybenzoxazine.	86

FIGURE	PAGE
5.4 Adsorption/desorption isotherms of carbon materials from PBZ prepared by two preparation methods: a conventional technique and a sol-gel technique by DETA as precursor (at 40 °C and 1 bar).	94
5.5 Adsorption/desorption isotherms of carbon materials from PBZ prepared by two preparation methods: a conventional technique and a sol-gel technique by DETA as precursor (at 40 °C and 1 bar).	95
5.6 Adsorption/desorption isotherms of carbon aerogels at different benzoxazine concentrations by DETA as precursor (at 40 °C and 1 bar).	96
5.7 Adsorption/desorption isotherms of carbon aerogels at different benzoxazine concentrations by PEHA as precursor (at 40 °C and 1 bar).	97
5.8 Adsorption/desorption isotherms of activated carbons derived from PBZ by DETA and PEHA as amine precursors (at 40 °C and 1 bar).	98
5.9 Adsorption/desorption isotherms of carbon aerogels from 30 wt% of benzoxazine solution by DETA and PEHA as amine precursors (at 40 °C and 1 bar).	98
5.10 Adsorption/desorption isotherms of carbon aerogels from 30 wt% of benzoxazine solution with different activation temperatures of 800 and 900 °C by DETA as precursor (at 40 °C and 1 bar).	99
5.11 Adsorption/desorption isotherms of carbon aerogels from 30 wt% of benzoxazine solution with different activation temperatures of 800 and 900 °C by PEHA as precursor (at 40 °C and 1 bar)	100
5.12 Adsorption/desorption isotherms of carbon aerogels from 30 wt% of benzoxazine solution with and without non-ionic surfactant at activation temperature of 900 °C by DETA as precursor (at 40 °C and 1 bar).	101

FIGURE	PAGE
5.13 Adsorption/desorption isotherms of carbon aerogels from 30 wt% of benzoxazine solution with and without non-ionic surfactant at activation temperature of 900 °C by PEHA as precursor (at 40 °C and 1 bar).	102
5.14 Desorption isotherms of activated carbon from PBZ, carbon aerogels from 30 wt% of benzoxazine solution with and without non-ionic surfactant at activation temperature of 900 °C by DETA as precursor at 40 °C and 1 bar).	108
5.15 Desorption isotherms of activated carbon from PBZ, carbon aerogels from 30 wt% of benzoxazine solution with and without non-ionic surfactant at activation temperature of 900 °C by PEHA as precursor (at 40 °C and 1 bar).	108
5.16 Desorption isotherms of activated carbon from PBZ, carbon aerogels from 30 wt% of benzoxazine solution with and without non-ionic surfactant at activation temperature of 900 °C by DETA as precursor (at 75 °C and 1 bar).	109
5.17 Desorption isotherms of activated carbon from PBZ, carbon aerogels from 30 wt% of benzoxazine solution with and without non-ionic surfactant at activation temperature of 900 °C by PEHA as precursor (at 75 °C and 1 bar).	109
5.18 Desorption isotherms of activated carbon from PBZ, carbon aerogels from 30 wt% of benzoxazine solution with and without non-ionic surfactant at activation temperature of 900 °C by DETA as precursor (at 110 °C and 1 bar).	110
5.19 Desorption isotherms of activated carbon from PBZ, carbon aerogels from 30 wt% of benzoxazine solution with and without non-ionic surfactant at activation temperature of 900 °C by PEHA as precursor (at 110 °C and 1 bar).	110
B.1 FT-IR spectrum of the benzoxazine monomer by DETA as reactant.	124

FIGURE	PAGE
B.2 FT-IR spectrum of the benzoxazine monomer by PEHA as reactant.	124
B.3 FT-IR spectrum of polybenzoxazine by DETA as reactant.	125
B.4 FT-IR spectrum of polybenzoxazine by PEHA as reactant.	125
C.1 DSC thermograms of benzoxazine monomers by DETA and PEHA as reactants.	126
C.2 DSC thermograms of polybenzoxazines by DETA and PEHA as reactant.	126
C.3 DSC thermograms of (a) DETA-40wt% derived aerogel at 180 °C for 15 min, (b) DETA-40wt% derived aerogel at 180 °C for 30 min, and (c) DETA-40wt% derived aerogel at 180 °C for 45 min.	127
C.4 DSC thermograms of polybenzoxazine aerogels before curing step with DETA as reactant.	127
C.5 DSC thermograms of polybenzoxazine aerogels after curing step with DETA as reactant.	128
C.6 DSC thermograms of polybenzoxazine aerogels before curing step with PEHA as reactant.	128
C.7 DSC thermograms of polybenzoxazine aerogels after curing step with PEHA as reactant.	129
D.1 TGA thermograms of benzoxazine monomers with DETA and PEHA as amine reactants.	130
D.2 TGA thermograms of polybenzoxazine and polybenzoxazine aerogels with DETA as reactant.	130
D.3 TGA thermograms of polybenzoxazine and polybenzoxazine aerogels with PEHA as reactant.	131
D.4 TGA thermograms of PBZs derived from DETA and PEHA after heating up to 900 °C (with a heating rate of 20 °C/min).	131
D.5 TGA thermograms of PEG-PPG-PEG block copolymer after heating up to 900 °C (with heating rate of 20 °C/min).	132

FIGURE	PAGE
D.6 TGA thermograms of PBZ aerogels derived from DETA and PEHA with and without non-ionic surfactant (PEG-PPG-PEG block copolymer) after heating up to 900 °C (with heating rate of 20 °C/min).	132
G.1 C1s XPS spectra of DETA-derived polybenzoxazine.	136
G.2 O1s XPS spectra of DETA-derived polybenzoxazine.	136
G.3 N1s XPS spectra of DETA-derived polybenzoxazine.	137
G.4 C1s XPS spectra of a 30 wt% DETA-derived PBZ organic aerogel.	137
G.5 O1s XPS spectra of a 30 wt% DETA-derived PBZ organic aerogel.	138
G.6 N1s XPS spectra of a 30 wt% DETA-derived PBZ organic aerogel.	138
G.7 C1s XPS spectra of a 35 wt% DETA-derived PBZ organic aerogel.	139
G.8 O1s XPS spectra of a 35 wt% DETA-derived PBZ organic aerogel.	139
G.9 N1s XPS spectra of a 35 wt% DETA-derived PBZ organic aerogel.	140
G.10 C1s XPS spectra of a 40 wt% DETA-derived PBZ organic aerogel.	140
G.11 O1s XPS spectra of a 40 wt% DETA-derived PBZ organic aerogel.	141
G.12 N1s XPS spectra of a 40 wt% DETA-derived PBZ organic aerogel.	141
G.13 C1s XPS spectra of PEHA-derived polybenzoxazine.	142
G.14 O1s XPS spectra of PEHA-derived polybenzoxazine.	142
G.15 N1s XPS spectra of PEHA-derived polybenzoxazine.	143
G.16 C1s XPS spectra of a 30 wt% PEHA-derived PBZ organic aerogel.	143
G.17 O1s XPS spectra of a 30 wt% PEHA-derived PBZ organic aerogel.	144
G.18 N1s XPS spectra of a 30 wt% PEHA-derived PBZ organic aerogel.	144
G.19 C1s XPS spectra of a 35 wt% PEHA-derived PBZ organic aerogel.	145
G.20 O1s XPS spectra of a 35 wt% PEHA-derived PBZ organic aerogel.	145
G.21 N1s XPS spectra of a 35 wt% PEHA-derived PBZ organic aerogel.	146
G.22 C1s XPS spectra of a 40 wt% PEHA-derived PBZ organic aerogel.	146
G.23 O1s XPS spectra of a 40 wt% PEHA-derived PBZ organic aerogel.	147
G.24 N1s XPS spectra of a 40 wt% PEHA-derived PBZ organic aerogel.	147
G.25 C1s XPS spectra of activated carbon from DETA-derived PBZ.	148
G.26 O1s XPS spectra of activated carbon from DETA-derived PBZ.	148

FIGURE	PAGE
G.27 N1s XPS spectra of activated carbon from DETA-derived PBZ.	149
G.28 C1s XPS spectra of a 30 wt% DETA-derived PBZ carbon aerogel.	149
G.29 O1s XPS spectra of a 30 wt% DETA-derived PBZ carbon aerogel.	150
G.30 N1s XPS spectra of a 30 wt% DETA-derived PBZ carbon aerogel.	150
G.31 C1s XPS spectra of a 35 wt% DETA-derived PBZ carbon aerogel.	151
G.32 O1s XPS spectra of a 35 wt% DETA-derived PBZ carbon aerogel.	151
G.33 N1s XPS spectra of a 35 wt% DETA-derived PBZ carbon aerogel.	152
G.34 C1s XPS spectra of a 40 wt% DETA-derived PBZ carbon aerogel.	152
G.35 O1s XPS spectra of a 40 wt% DETA-derived PBZ carbon aerogel.	153
G.36 N1s XPS spectra of a 40 wt% DETA-derived PBZ carbon aerogel.	153
G.37 C1s XPS spectra of activated carbon from PEHA-derived PBZ.	154
G.38 O1s XPS spectra of activated carbon from PEHA-derived PBZ.	154
G.39 N1s XPS spectra of activated carbon from PEHA-derived PBZ.	155
G.40 C1s XPS spectra of a 30 wt% PEHA-derived PBZ carbon aerogel.	155
G.41 O1s XPS spectra of a 30 wt% PEHA-derived PBZ carbon aerogel.	156
G.42 C1s XPS spectra of a 35 wt% PEHA-derived PBZ carbon aerogel.	156
G.43 C1s XPS spectra of a 35 wt% PEHA-derived PBZ carbon aerogel.	157
G.44 O1s XPS spectra of a 35 wt% PEHA-derived PBZ carbon aerogel.	157
G.45 N1s XPS spectra of a 35 wt% PEHA-derived PBZ carbon aerogel.	158
G.46 C1s XPS spectra of a 40 wt% PEHA-derived PBZ carbon aerogel.	158
G.47 O1s XPS spectra of a 40 wt% PEHA-derived PBZ carbon aerogel.	159
G.48 N1s XPS spectra of a 40 wt% PEHA-derived PBZ carbon aerogel.	159
G.49 C1s XPS spectra of activated carbon from DETA-derived PBZ at activation temperature of 900 °C.	160
G.50 O1s XPS spectra of activated carbon from DETA-derived PBZ at activation temperature of 900 °C.	160
G.51 N1s XPS spectra of activated carbon from DETA-derived PBZ at activation temperature of 900 °C.	161
G.52 C1s XPS spectra of a 30 wt% DETA-derived PBZ carbon aerogel at activation temperature of 900 °C.	161

FIGURE	PAGE
G.53 O1s XPS spectra of a 30 wt% DETA-derived PBZ carbon aerogel at activation temperature of 900 °C.	162
G.54 N1s XPS spectra of a 30 wt% DETA-derived PBZ carbon aerogel at activation temperature of 900 °C.	162
G.55 C1s XPS spectra of a 30 wt% DETA-derived PBZ carbon aerogel loading with non-ionic surfactant at activation temperature of 900 °C.	163
G.56 O1s XPS spectra of a 30 wt% DETA-derived PBZ carbon aerogel loading with non-ionic surfactant at activation temperature of 900 °C.	163
G.57 N1s XPS spectra of a 30 wt% DETA-derived PBZ carbon aerogel loading with non-ionic surfactant at activation temperature of 900 °C.	164
G.58 C1s XPS spectra of activated carbon from PEHA-derived PBZ at activation temperature of 900 °C.	164
G.59 O1s XPS spectra of activated carbon from PEHA-derived PBZ at activation temperature of 900 °C.	165
G.60 N1s XPS spectra of activated carbon from PEHA-derived PBZ at activation temperature of 900 °C.	165
G.61 C1s XPS spectra of a 30 wt% PEHA-derived PBZ carbon aerogel at activation temperature of 900 °C.	166
G.62 O1s XPS spectra of a 30 wt% PEHA-derived PBZ carbon aerogel at activation temperature of 900 °C.	166
G.63 N1s XPS spectra of a 30 wt% PEHA-derived PBZ carbon aerogel at activation temperature of 900 °C.	167
G.64 C1s XPS spectra of a 30 wt% PEHA-derived PBZ carbon aerogel loading with non-ionic surfactant at activation temperature of 900 °C.	167

FIGURE	PAGE
G.65 O1s XPS spectra of a 30 wt% PEHA-derived PBZ carbon aerogel loading with non-ionic surfactant at activation temperature of 900 °C.	168
G.66 N1s XPS spectra of a 30 wt% PEHA-derived PBZ carbon aerogel loading with non-ionic surfactant at activation temperature of 900 °C.	168
H.1 Isotherm of a 30 wt% DETA-derived PBZ organic aerogel.	169
H.2 Barrett-Joyner-Halenda pore size distribution of a 30 wt% DETA-derived PBZ organic aerogel.	169
H.3 Horvath and Kawazoe pore size distribution of a 30 wt% DETA-derived PBZ organic aerogel.	170
H.4 Isotherm of a 35 wt% DETA-derived PBZ organic aerogel.	170
H.5 Barrett-Joyner-Halenda pore size distribution of a 35 wt% DETA-derived PBZ organic aerogel.	171
H.6 Horvath and Kawazoe pore size distribution of a 35 wt% DETA-derived PBZ organic aerogel.	171
H.7 Isotherm of a 40 wt% DETA-derived PBZ organic aerogel.	172
H.8 Barrett-Joyner-Halenda pore size distribution of a 40 wt% DETA-derived PBZ organic aerogel.	172
H.9 Horvath and Kawazoe pore size distribution of a 40 wt% DETA-derived PBZ organic aerogel.	173
H.10 Isotherm of a 30 wt% PEHA-derived PBZ organic aerogel.	173
H.11 Barrett-Joyner-Halenda pore size distribution of a 30 wt% PEHA-derived PBZ organic aerogel.	174
H.12 Horvath and Kawazoe pore size distribution of a 30 wt% PEHA-derived PBZ organic aerogel.	174
H.13 Isotherm of a 35 wt% PEHA-derived PBZ organic aerogel.	175
H.14 Horvath and Kawazoe pore size distribution of a 35 wt% PEHA-derived PBZ organic aerogel.	175
H.15 Isotherm of a 40 wt% PEHA-derived PBZ organic aerogel.	176

FIGURE	PAGE
H.16 Horvath and Kawazoe pore size distribution of a 40 wt% PEHA-derived PBZ organic aerogel.	176
H.17 Isotherm of activated carbon from DETA-derived PBZ.	177
H.18 Barrett-Joyner-Halenda pore size distribution of activated carbon from DETA-derived PBZ.	177
H.19 Horvath and Kawazoe pore size distribution of activated carbon from DETA-derived PBZ.	178
H.20 Isotherm of a 30 wt% DETA-derived PBZ carbon aerogel.	178
H.21 Barrett-Joyner-Halenda pore size distribution of a 30 wt% DETA-derived PBZ carbon aerogel.	179
H.22 Horvath and Kawazoe pore size distribution of a 30 wt% DETA-derived PBZ carbon aerogel.	179
H.23 Isotherm of a 35 wt% DETA-derived PBZ carbon aerogel.	180
H.24 Barrett-Joyner-Halenda pore size distribution of a 35 wt% DETA-derived PBZ carbon aerogel.	180
H.25 Horvath and Kawazoe pore size distribution of a 35 wt% DETA-derived PBZ carbon aerogel.	181
H.26 Isotherm of a 40 wt% DETA-derived PBZ carbon aerogel.	181
H.27 Barrett-Joyner-Halenda pore size distribution of a 40 wt% DETA-derived PBZ carbon aerogel.	182
H.28 Horvath and Kawazoe pore size distribution of a 40 wt% DETA-derived PBZ carbon aerogel.	182
H.29 Isotherm of activated carbon from PEHA-derived PBZ.	183
H.30 Barrett-Joyner-Halenda pore size distribution of activated carbon from PEHA-derived PBZ.	183
H.31 Horvath and Kawazoe pore size distribution of activated carbon from PEHA-derived PBZ.	184
H.32 Isotherm of a 30 wt% PEHA-derived PBZ carbon aerogel.	184
H.33 Barrett-Joyner-Halenda pore size distribution of a 30 wt% PEHA-derived PBZ carbon aerogel.	185

FIGURE	PAGE
H.34 Horvath and Kawazoe pore size distribution of a 30 wt% PEHA-derived PBZ carbon aerogel.	185
H.35 Isotherm of a 35 wt% PEHA-derived PBZ carbon aerogel.	186
H.36 Barrett-Joyner-Halenda pore size distribution of a 35 wt% PEHA-derived PBZ carbon aerogel.	186
H.37 Horvath and Kawazoe pore size distribution of a 35 wt% PEHA-derived PBZ carbon aerogel.	187
H.38 Isotherm of a 40 wt% PEHA-derived PBZ carbon aerogel.	187
H.39 Barrett-Joyner-Halenda pore size distribution of a 40 wt% PEHA-derived PBZ carbon aerogel.	188
H.40 Horvath and Kawazoe pore size distribution of a 40 wt% PEHA-derived PBZ carbon aerogel.	188
H.41 Isotherm of activated carbon from DETA-derived PBZ at activation temperature of 900 °C.	189
H.42 Barrett-Joyner-Halenda pore size distribution of activated carbon from DETA-derived PBZ at activation temperature of 900 °C.	189
H.43 Horvath and Kawazoe pore size distribution of activated carbon from DETA-derived PBZ at activation temperature of 900 °C.	190
H.44 Isotherm of a 30 wt% DETA-derived PBZ carbon aerogel at activation temperature of 900 °C.	190
H.45 Horvath and Kawazoe pore size distribution of a 30 wt% DETA-derived PBZ carbon aerogel at activation temperature of 900 °C.	191
H.46 Isotherm of a 30 wt% DETA-derived PBZ carbon aerogel loading with non-ionic surfactant at activation temperature of 900 °C.	191
H.47 Barrett-Joyner-Halenda pore size distribution of a 30 wt% DETA-derived PBZ carbon aerogel loading with non-ionic surfactant at activation temperature of 900 °C.	192
H.48 Horvath and Kawazoe pore size distribution of a 30 wt% DETA-derived PBZ carbon aerogel loading with non-ionic surfactant at activation temperature of 900 °C.	192

FIGURE	PAGE
H.49 Isotherm of activated carbon from PEHA-derived PBZ at activation temperature of 900 °C.	193
H.50 Barrett-Joyner-Halenda pore size distribution of activated carbon from PEHA-derived PBZ at activation temperature of 900 °C.	193
H.51 Horvath and Kawazoe pore size distribution of activated carbon from PEHA-derived PBZ at activation temperature of 900 °C.	194
H.52 Isotherm of a 30 wt% PEHA-derived PBZ carbon aerogel at activation temperature of 900 °C.	194
H.53 Barrett-Joyner-Halenda pore size distribution of a 30 wt% PEHA-derived PBZ carbon aerogel at activation temperature of 900 °C.	195
H.54 Horvath and Kawazoe pore size distribution of a 30 wt% PEHA-derived PBZ carbon aerogel at activation temperature of 900 °C.	195
H.55 Isotherm of a 30 wt% PEHA-derived PBZ carbon aerogel loading with non-ionic surfactant at activation temperature of 900 °C.	196
H.56 Barrett-Joyner-Halenda pore size distribution of a 30 wt% PEHA-derived PBZ carbon aerogel loading with non-ionic surfactant at activation temperature of 900 °C.	196
H.57 Horvath and Kawazoe pore size distribution of a 30 wt% PEHA-derived PBZ carbon aerogel loading with non-ionic surfactant at activation temperature of 900 °C.	197
I.1 Adsorption/desorption isotherms of DETA-derived activated carbons at activating temperature of 800 °C (at 40, 75, 110 °C and 1 bar).	198
I.2 Adsorption/desorption isotherms of carbon aerogels from 30 wt% DETA-derived PBZ at activating temperature of 800 °C (at 40, 75, 110 °C and 1 bar).	198
I.3 Adsorption/desorption isotherms of carbon aerogels from 35 wt% DETA-derived PBZ at activating temperature of 800 °C (at 40, 75, 110 °C and 1 bar).	199

FIGURE		PAGE
I.4	Adsorption/desorption isotherms of carbon aerogels from 40 wt% DETA-derived PBZ at activating temperature of 800 °C (at 40, 75, 110 °C and 1 bar).	199
I.5	Adsorption/desorption isotherms of PEHA-derived activated carbons at activating temperature of 800 °C (at 40, 75, 110 °C and 1 bar).	200
I.6	Adsorption/desorption isotherms of carbon aerogels from 30 wt% PEHA-derived PBZ at activating temperature of 800 °C (at 40, 75, 110 °C and 1 bar).	200
I.7	Adsorption/desorption isotherms of carbon aerogels from 35 wt% PEHA-derived PBZ at activating temperature of 800 °C (at 40, 75, 110 °C and 1 bar).	201
I.8	Adsorption/desorption isotherms of carbon aerogels from 40 wt% PEHA-derived PBZ at activating temperature of 800 °C (at 40, 75, 110 °C and 1 bar).	201
I.9	Adsorption/desorption isotherms of DETA-derived activated carbons at activating temperature of 900 °C (at 40, 75, 110 °C and 1 bar).	202
I.10	Adsorption/desorption isotherms of carbon aerogels from 30 wt% DETA-derived PBZ at activating temperature of 900 °C (at 40, 75, 110 °C and 1 bar).	202
I.11	Adsorption/desorption isotherms of carbon aerogels from 30 wt% DETA-derived PBZ loading non-ionic surfactant at activating temperature of 900 °C (at 40, 75, 110 °C and 1 bar).	203
I.12	Adsorption/desorption isotherms of PEHA-derived activated carbons at activating temperature of 900 °C (at 40, 75, 110 °C and 1 bar).	203

FIGURE	PAGE
I.13 Adsorption/desorption isotherms of carbon aerogels from 30 wt% PEHA-derived PBZ at activating temperature of 900 °C (at 40, 75, 110 °C and 1 bar).	204
I.14 Adsorption/desorption isotherms of carbon aerogels from 30 wt% PEHA-derived PBZ loading non-ionic surfactant at activating temperature of 900 °C (at 40, 75, 110 °C and 1 bar).	204
J.1 SEM images of (a) fully cured DETA-derived PBZ aerogel at 20 wt%, (b) 25 wt%, and (c) 30 wt% of monomer solutions.	205
J.2 SEM images of (a) activated carbon from DETA-derived PBZ and (b) activated carbon from PEHA-derived PBZ at activating temperature of 800 °C.	205
J.3 SEM images of (a) DETA-derived PBZ carbon aerogel at 30 wt%, (b) 30 wt%, (c) 35 wt%, (d) 35 wt%, (e) 40 wt%, and (f) 40 wt% of monomer solutions at activating temperature of 800 °C; low magnification for (a), (c), and (e); high magnification for (b), (d), and (f).	206
J.4 SEM images of (a) PEHA-derived PBZ carbon aerogel at 30 wt%, (b) 30 wt%, (c) 35 wt%, (d) 35 wt%, (e) 40 wt%, and (f) 40 wt% of monomer solutions at activating temperature of 800 °C; low magnification for (a), (c), and (e); high magnification for (b), (d), and (f).	207
J.5 SEM images of (a) activated carbon from DETA-derived PBZ, (b) activated carbon from PEHA-derived PBZ, (c) DETA-derived PBZ carbon aerogel at 30 wt% (d) PEHA-derived PBZ carbon aerogel at 30 wt%, (e) DETA-derived PBZ carbon aerogel at 30 wt% loading non-ionic surfactant, and (f) PEHA-derived PBZ carbon aerogel at 30 wt% loading non-ionic surfactant at activating temperature of 900 °C.	208